JOURNAL OF Applied Polymer SCIENCE

Superhydrophobic Durable Coating Based on UV-Photoreactive Silica Nanoparticles

Tehila Nahum,[1] Hanna Dodiuk,[1] Anna Dotan,[1] Shmuel Kenig,[1] Jean Paul Lellouche[2]

[1]Department of Plastics Engineering, The Pernick Faculty of Engineering, Shenkar College of Engineering and Design, Ramat Gan 52526, Israel

[2]Department of Chemistry, Nanomaterials Research Center, Institute of Nanotechnology and Advanced Materials, Bar-Ilan University, Ramat Gan 52900, Israel

Correspondence to: T. Nahum (E-mail: tehilanah@gmail.com)

ABSTRACT: Superhydrophobic surfaces can be obtained by tailoring both the chemistry and roughness topography, mimicking the Lotus leaf characteristics. Most of the synthetic superhydrophobic surfaces reported have been composed of micro and nanoparticles (NPs) embedded in polymer-based coatings. The particles which tailor the topography are bonded to the base polymers by weak secondary forces. Consequently, the topography integrity is highly affected by handling and surface drag making them unsuitable for long term applications. This work is focused on promoting covalent bonding between the NPs and the base polymer to obtain durable superhydrophobic surfaces. The rough topography was achieved by ultraviolet (UV) curing of SiO_2 NPs containing a photoreactive benzophenone moiety in addition to methylated fumed silica NPs which can bind covalently to the polymer base coating, on UV radiation. The hydrophobic chemistry was obtained by fluoroalkylsilane top coating. Coating durability was evaluated using surface air drag and accelerated weathering conditions (UV radiation, humidity and temperature). Results indicated that the proposed approach resulted in superhydrophobic surfaces having high contact angle (>150°) and low sliding angle (<10°) with improved long term durability. © 2014 Wiley Periodicals, Inc. J. Appl. Polym. Sci. **2014**, *131*, 41122.

KEYWORDS: hydrophobic coatings; silica nanoparticles; ultraviolet curing

Received 15 January 2014; accepted 8 June 2014

DOI: 10.1002/app.41122

INTRODUCTION

Superhydrophobic surfaces with static contact angles above 150° and sliding angles below 10°[1] allowing easy rolling of water droplets along the surface have been studied for a variety of applications such as: self-cleaning,[2,3] anticorrosion,[4] antipollution,[5] oil/water separation,[6,7] self-healing,[8] and ice repellant surfaces.[9–14] It is well known that the wettability of hydrophobic surfaces can be altered with hierarchical surface topography (both nanometer and micrometer-sized) and hydrophobic chemistry (fluorine, alkane, or silicone based moieties) mimicking the lotus leaf.[7,15–20]

There are several approaches for creating superhydrophobic surfaces: (1) top down approach is obtained by breaking down of a system to gain insight into its compositional subsystems, and includes plasma etching[21,22] and lithography[23,24]; (2) bottom up approach is obtained by integrating systems to give rise to more complex systems and can be achieved using common methods such as sol gel,[25] microphase separation,[26,27] spray coating,[28] electrochemical deposition,[7,29] and nanoparticles (NPs) assembly[30,31]; (3) Third approach is obtained by a combination of top down and bottom up approaches using templating process.[32–35] This process is usually based on a soft and deformable material, that is, used to cast and replicate the structures of the template surface. Silica NPs are widely used to control surface roughness using different coating methods such as spin coating, dip coating, and spray coating. There are many self-assembly methods used to fabricate superhydrophobic surfaces but most of them lose their rough topography under harsh conditions and thus are unsuitable for long term applications.[24,25,30,36–38] Rios et al.[3] developed solvent-bonding technique for the NPs and enhanced the mechanical stability of superhydrophobic surfaces but still the durability decreased with increasing mechanical attrition. In Xiu et al.[39] work, superhydrophobic surfaces were prepared using silica NPs. They showed that the microsurface roughness was reduced due to mechanical abrasion. She et al.[40] investigated the mechanical durability of anticorrosion superhydrophobic surfaces on a magnesium alloy using the scratch test. The result showed that the contact angle (CA) was maintained above 150° while the sliding angle (SA)

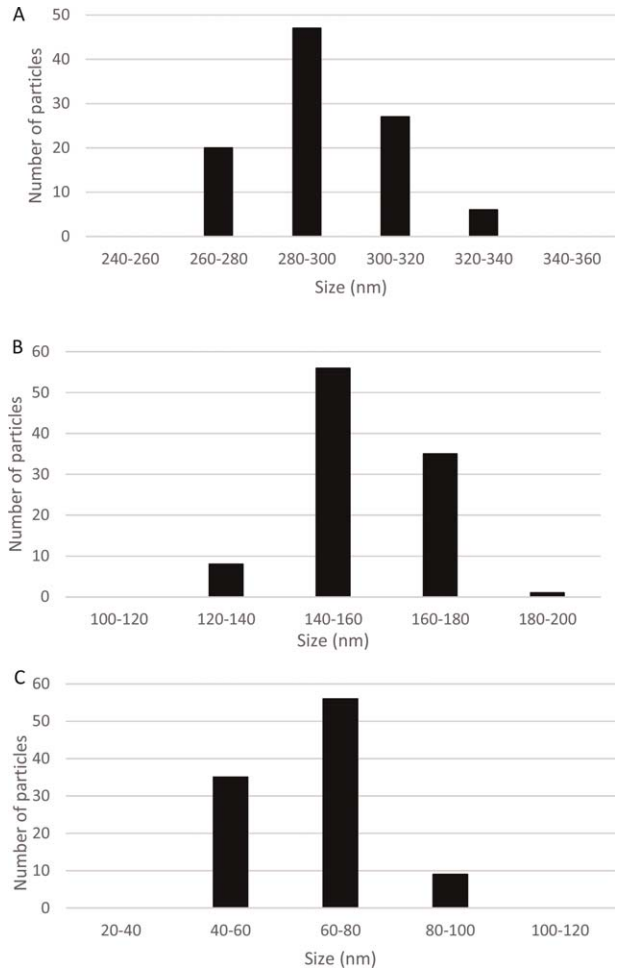

Figure 1. TEM images and size distribution histogram of A) SiO_2@BPh NPs with calculated average size of 294 ± 15 nm. B) SiO_2@BPh NPs with calculated average size of 156 ± 12 nm. C) SiO_2@BPh NPs with calculated average size of 65 ± 11 nm.

increased after abrasion. Other studies also addressed the mechanical robustness under environmental and UV radiation conditions,[41] thermal,[25] chemical,[42] and in water enviroments.[43] In all cases, the loss of roughness led to unstable Cassie state and increased the area of contact between the water droplets and the surface.[44] The creation of covalent bonding between the NPs and the substrate can ensure enhanced endurance and its implementation in practical applications.[45] The objective of this work is to study the effect of ultraviolet (UV) chemistry on covalent bonding formation between silica NPs to UV cured polymers to obtain durable superhydrophobic coatings.

METHODOLGY

Two basic features have to be combined to obtain durable superhydrophobicity. Thus, it is proposed to investigate the possibility to obtain robust hydrophobic topography by covalently binding silica NPs to a polymer base coating.[45,46] Furthermore, a top layer of Fluor containing film will be studied for superhydrophobic chemistry. Accordingly, a three layer structure could be obtained as shown schematically in Scheme 1. Two silica based NPs were evaluated: SiO_2 NPs crowned with UV reactive functional groups and methylated fumed silica NPs. The studied Fluor top layer was based on Fluorosilane. A variety of mechanical abrasion methods as well as exposure to accelerated weathering were applied to study the durability of the layered coating with respect to its superhydrophobic characteristics.

EXPERIMENTAL

Based on the above methodology, the experimental study comprised a few stages: in the first stage, the UV reactive moiety composed of BPhTES (4-benzoyl-N-(3-(triethoxysilyl)propyl) benzamide 3) was synthesized, followed by a second stage where the UV reactive BPhTES was reacted with TEOS (tetraethyl orthosilicate) to produce UV reactive silica NPs. The layered coating was prepared using a base polymer, UV reactive silica NPs, methylated silica NPs, and Fluorosilane top layer.

Materials

Urethane acrylate (UV) (NOA61 Norland Products incorporated) was used as the base coating. 4-benzoylbenzoic acid, 1,1-carbonyl-diimidazole (CDI), 3-amino-propyltriethoxysilane (APTES), tetraethyl orthosilicate (TEOS; Sigma Aldrich) was used for synthesis of the UV reactive silica NPs. Methylated fumed silica (CAB-O-SIL TS-720 – CABOT) was combined with the UV reactive NPs. Fluoroalkylsilane (F8263 Evonick Industries) was used as the top layer.

Synthetic Methods

Synthesis of BPhTES (4-benzoyl-N-(3-(triethoxysilyl)propyl) benzamide 3). BPhTES was synthesized as a first stage for the preparation of the hybrid photo reactive nanosilica particles.[46] 4-benzoylbenzoic acid (2.26 g, 10 mmol) and CDI (162 g, 10 mmol) were dissolved in dry THF (40 ml) in a two neck bottom flask equipped with drying tube. The solution was stirred at RT for 2 hr and then APTES (2.32 ml, 10 mmol) was added to the reaction. The reaction was stirred continuous for 24 hr at the same temperature. After reaction completion (TLC testing), the medium was concentrated in vacuum achieving a yellowish solid. Purification step was done by flash chromatography on silica gel (eluent: acetone/*n*-hexane: 85/15) to give 69% yield (2.98 g, 6.94 mmol).

Preparation of Hybrid Silica NPs

BPhTES (0.76 mmol) was added to a solution of EtOH (45 ml) with TEOS (1.55 ml, 6.84 mmol) under vigorous stirring at RT.[46] Then, water (2.75 ml) and NH_4OH 28% (1.2 ml) were added to the reaction. The reaction proceeded for 6 hr. Isolation of the NPs was carried out by centrifugation (15,000 rpm, 0° C, 20 min) then the surfactant was removed and SiO_2@BPh NPs were dispersed in ethanol (30 ml) using a bath sonicator. All

Scheme 1. Schematic presentation of proposed three layer composite superhydrophobic coating. [Color figure can be viewed in the online issue, which is available at wileyonlinelibrary.com.]

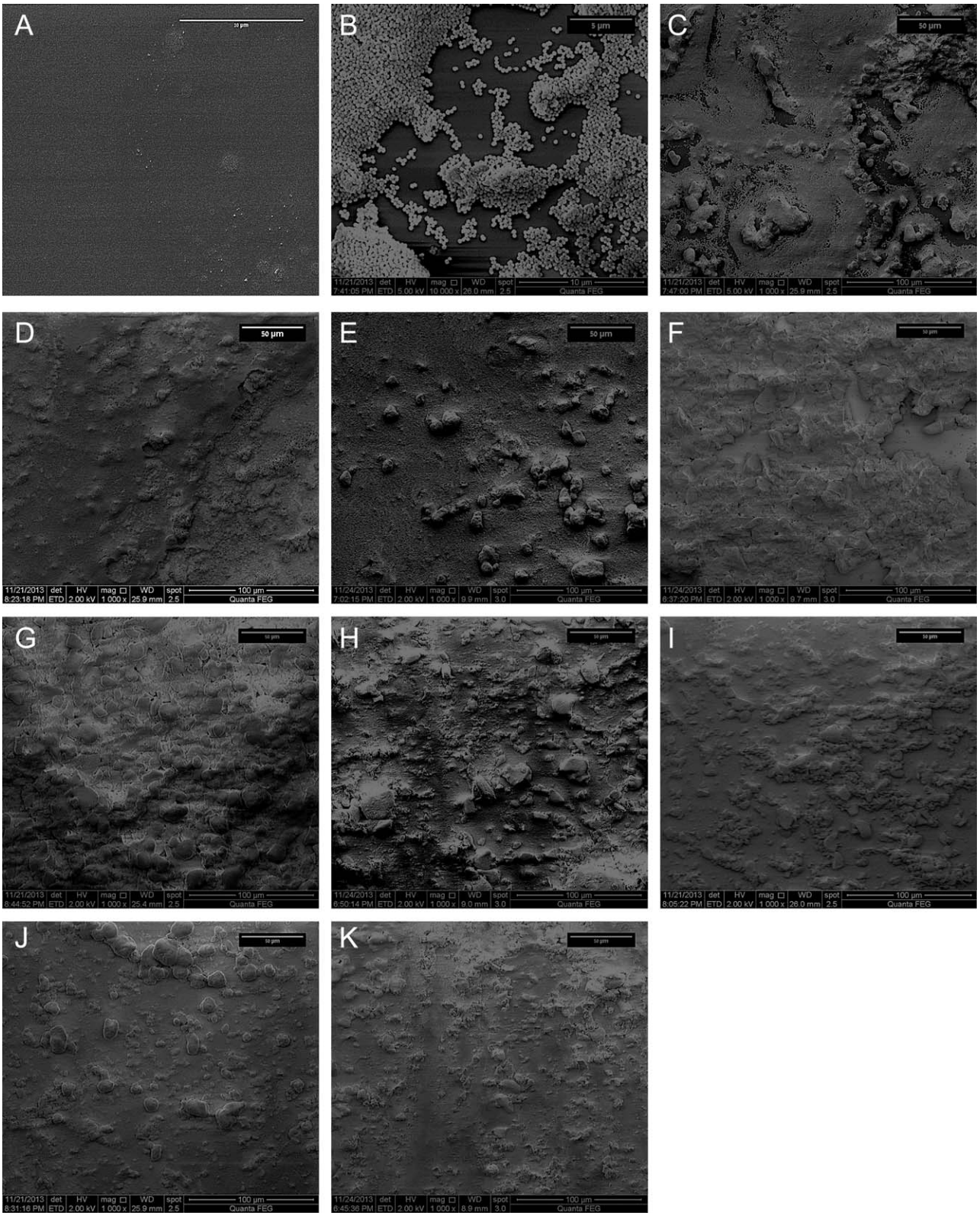

Figure 2. SEM topography image of A) UA neat. B) Magnification: SEM topography image of UA + SiO_2@BPh294 NPs. C) UA + SiO_2@BPh294 NPs. Rough surface was obtained D) UA+ SiO_2@BPh294 NPs + methylated fumed silica. E) UA+ SiO_2@BPh294 NPs + Hydrophobic fumed silica + FAS. F) UA+ SiO_2@BPh156 NPs. G) UA + SiO_2@BPh156 NPs + methylated fumed silica. H) UA + SiO_2@BPh156 NPs + methylated fumed silica + FAS. I) UA + SiO_2@BPh65 NPs. J) UA+ SiO_2@BPh65 NPs + methylated fumed silica. K) UA + SiO_2@BPh156 NPs + methylated fumed silica + FAS.

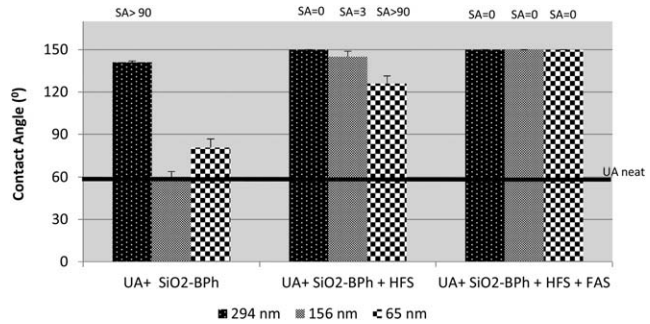

Figure 3. Contact angle and sliding angle measurements for all layers. Sliding angle measured only for hydrophobic surfaces.

process was repeated five times. The purified SiO_2@BPh NPs were dried in a vacuum oven overnight to remove residual solvent. Lastly, dispersion of 2% wt SiO_2@BPh NPs in ethyl acetate was prepared using a bath sonicator for 20 min. Synthesis of higher particle size were prepared by the same procedure using water volume of 3.65 and 7.57 ml and NH_3 volume of 5.67 and 9 ml, respectively.

Preparation of Methylated Fumed Silica Dispersion. Ultrahydrophobic TS-720 (0.5% wt) was dispersed in ethyl acetate using a bath sonicator for 30 min.

Coating Preparation. First layer: 300 µl diluted urethane acrylate were spin coated (Speed 1 : 800 rpm 30 sec. Speed 2 : 1 min, 1500 rpm) on glass substrate and UV irradiated for 30 sec. Second layer: The UA coating was immersed in a dispersion of 2% wt of SiO_2@BPh in ethyl acetate (10 ml) for 2 min. Then, the substrate was UV irradiated for 1 min to allow partial chemical bonding. Third layer: The substrate was immersed in a methylated fumed silica dispersion for 2 min and UV irradiated for another 1 min to ensure maximum conversion and bonding. Forth layer: The substrate was immersed in floroalkysilane solution for 2 min and then dried at 80°C for 2 hr.

Bonding Strength. The bonding of the silica NPs to the base polymer coating was evaluated using high velocity air flow. The drag force of the flowing air was calculated from eq. (1).

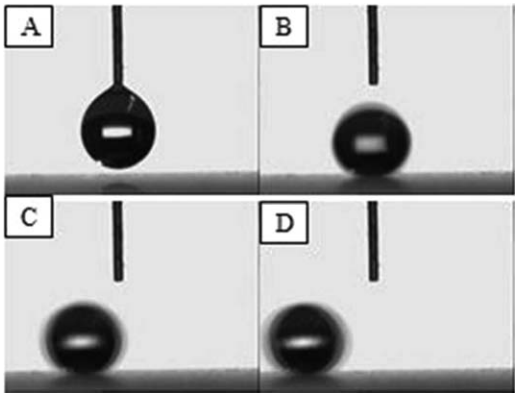

Figure 4. Water drop sliding on a superhydrophobic surface. Horizontal plane.

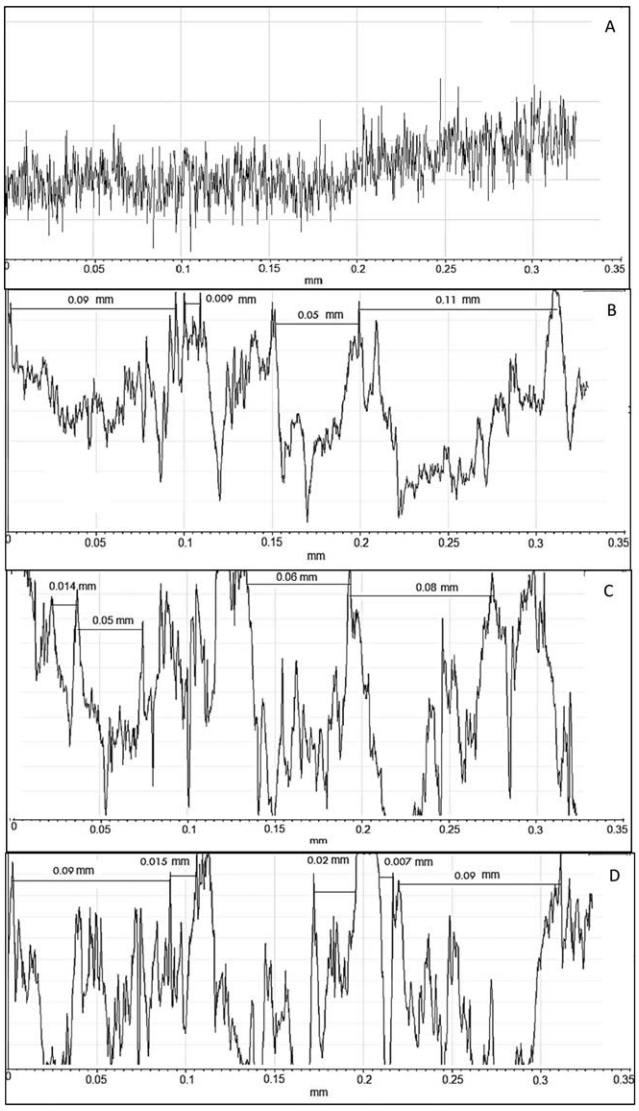

Figure 5. Surface profile of A) UA neat, B) FC294, C) FC156, and D) FC65.

$$F_D = \frac{1}{2}\rho V^2 C_D A \quad (1)$$

Where F_D is the drag force component in the direction of the flow velocity, ρ is the density of air at room temperature and atmospheric pressure taken from the ideal gas equation (kg/m^3). A is the bonding area [for spherical geometry is $(4\pi r^2)$] and V is the air velocity reading from the anemometer (m/s). C_D is the drag coefficient related to the object's geometry and is function of Reynolds number.[47] Reynolds number is defined in the following Equation:

$$\mathrm{Re} = \frac{\rho VD}{\mu} = \frac{VL}{v} \quad (2)$$

Where V is the mean air velocity (m/s), L is a characteristic linear dimension, µ is the dynamic viscosity of the fluid (Pa s or N s/m^2), v the kinematic viscosity ($v = \frac{\mu}{\rho}$) (m^2/s) and ρ is the density of air (kg/m^3).

Characterization. Transmission Electron Microscope (TEM) images were taken (120 kV FEI, Tecani G12 BIOTWIN). Samples

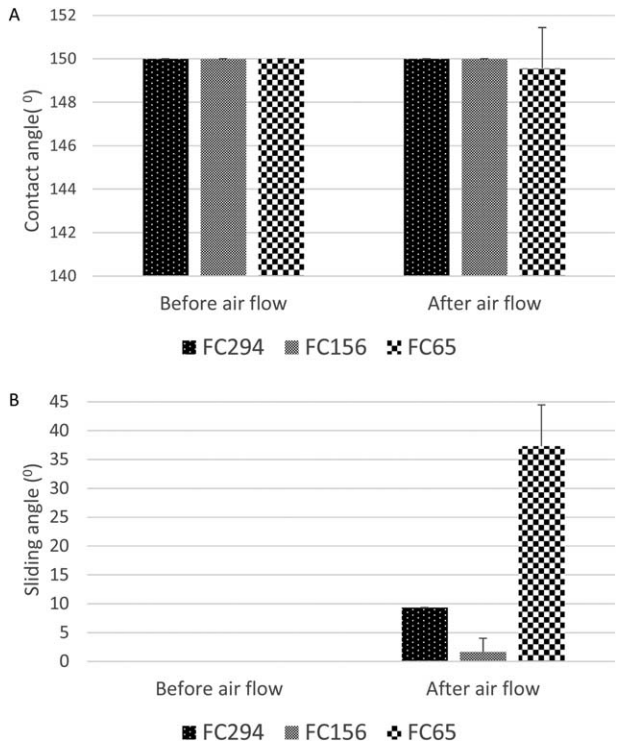

Figure 6. A) Contact angles measurements for FC294, FC156, and FC65 before and after air flow of 82 m/sec. B) Sliding angles measurements for FC294, FC156, and FC65 before and after air flow of 82 m/sec.

were prepared on Formvar/Carbon 400 m mesh Cu grids by applying an ethanol solution of the particles. The average size of NPs was determined by measuring 100 NPs from the TEM images using the ImageJ software. UV irradiations were carried out using a special UV lamp (Ultracure-200 1000w from Hernon Manufacturing). Environmental scanning electron microscope (E-SEM) images were taken (*Quanta* Field Emission Gun (FEG)) for structure analysis. Samples were prepared on Cu pellets by tape bonding of the coated glass substrate. Spin coater (Chemat Technology, KW-4A) was used to enable uniform distribution of the polymer and NPs layers. The contact angle was measured by a sessile drop, using contact angle analyzer (OCA 20, Dataphysics Instruments GmbH, Germany). Deionized and ultrafiltered water (0.2 μm filter) was used for the measurements. The sliding angle was measured using a tilting unit (TBU90E, Dataphysics Instrument GmbH) incorporated into the contact angle analyzer. A drop was deposited on the horizontal substrate and after equilibrium the substrate plane was tilted at a rate of 100°/min until the onset of drop motion. Contact angles were measured using 5 μL water drops and sliding angles were measured using 30 μL water drops. Light transmission (LT) and haze characteristics were measured using a Hazemeter (BYK Gardner, Germany) following ASTM D1003 procedure. Outdoor durability was evaluated with a UV accelerated weathering chamber (Q-Panel) according to ASTM D4329 incorporating UV radiation, moisture, and heat. In this work, samples were exposed to accelerated weathering chamber for up to 500 hr using UVA 340 fluorescent lamps with a cycle comprising 8 hr radiation at 60° C and 4 hr condensation at 50°C (ASTM D4329—Cycle A). Samples were removed from the chamber at 100, 200, 300, and 500 hr, evaluated, and returned to the chamber again. Evaluation of the coating resistance to air drag was carried out by placing an air gun of 300 km/hr at a fixed distance from the sample. An anemometer was placed at the end of the sample to measure the velocity of air passing along the sample. Surface profile characterization was made using IP- Image procession and data analyzer version 2.1.

RESULTS AND DISCUSSION

In a previous study,[45] the functionalization of silica NPs by photo reactive benzophenone (BP) groups was carried out in order to covalently bond the NPs to polymer substrates with the objective to obtain durable coatings. The results have shown enhanced stability of the resultant hydrophobic coating by a layer of SiO_2@BPh NPs and a top layer of fluoroalkylsilane. To impart superhydrophobic characteristics, an additional layer comprising methylated fumed silica was added. On UV radiation the activated SiO_2@BPh NPs can interact with the C—H bond in the methyl terminated groups of the fumed silica NPs to yield covalent bonding. The methylated fumed silica NPs can increase both surface roughness and hydrophobic characteristics. In addition, larger NPs based on SiO_2@BPh were incorporated to increase surface roughness.

TEM images confirmed the spherical morphology of the SiO_2@BPh NPs having an average size of 294 ± 15 nm, 156 ± 12 nm, and 65 ± 11 nm, respectively (Figure 1). Corresponding particles distribution histograms are shown.

The proposed mechanism of the photochemical reaction between SiO_2@BPh NPs and methylated fumed silica is illustrated in Scheme 2. The BP reactive species can react with C—H bonds of the methyl groups through hydrogen abstraction leading to the formation of radicals on the hydrophobic fumed silica and on BP triplets culminating with bonding.

Topographies of the neat UA and NPs containing coating were investigated using SEM (Figure 2). Neat UA coatings showed smooth surface while all NPS containing coatings have shown nonuniform roughness morphologies. A close look at the UA + SiO_2@BPh294 NPs surface [Figure 2(B)] reveals that SiO_2@BPh NPs create both small and large aggregations that led to higher surface roughness.

Contact angle measurements showed that hydrophobic surfaces can be obtained using the rough layer of SiO_2@BPh294 with CA above 90° while SiO_2@BPh156 and SiO_2@BPh65 have led to hydrophilic surfaces with CA below 90° (Figure 3). These results indicate that above a critical particle size and corresponding roughness a significant increase in hydrophobicity was obtained even without hydrophobic chemistry. However, to achieve superhydrophobicity with higher CA ($CA > 150°$) and lower SA ($SA < 10°$), (see Figure 4), a hydrophobic top layer should be incorporated. The addition of the fluorosilane top layer led to superhydrophobicity of all surfaces with LT of 87%.

The effect of roughness texture such as pillar size, height, and spacing on wettability was studied elsewhere.[19,48] It was shown that the major effect on sliding angle was due to pillar spacing. In this work, the spacing between the peaks of the surface was

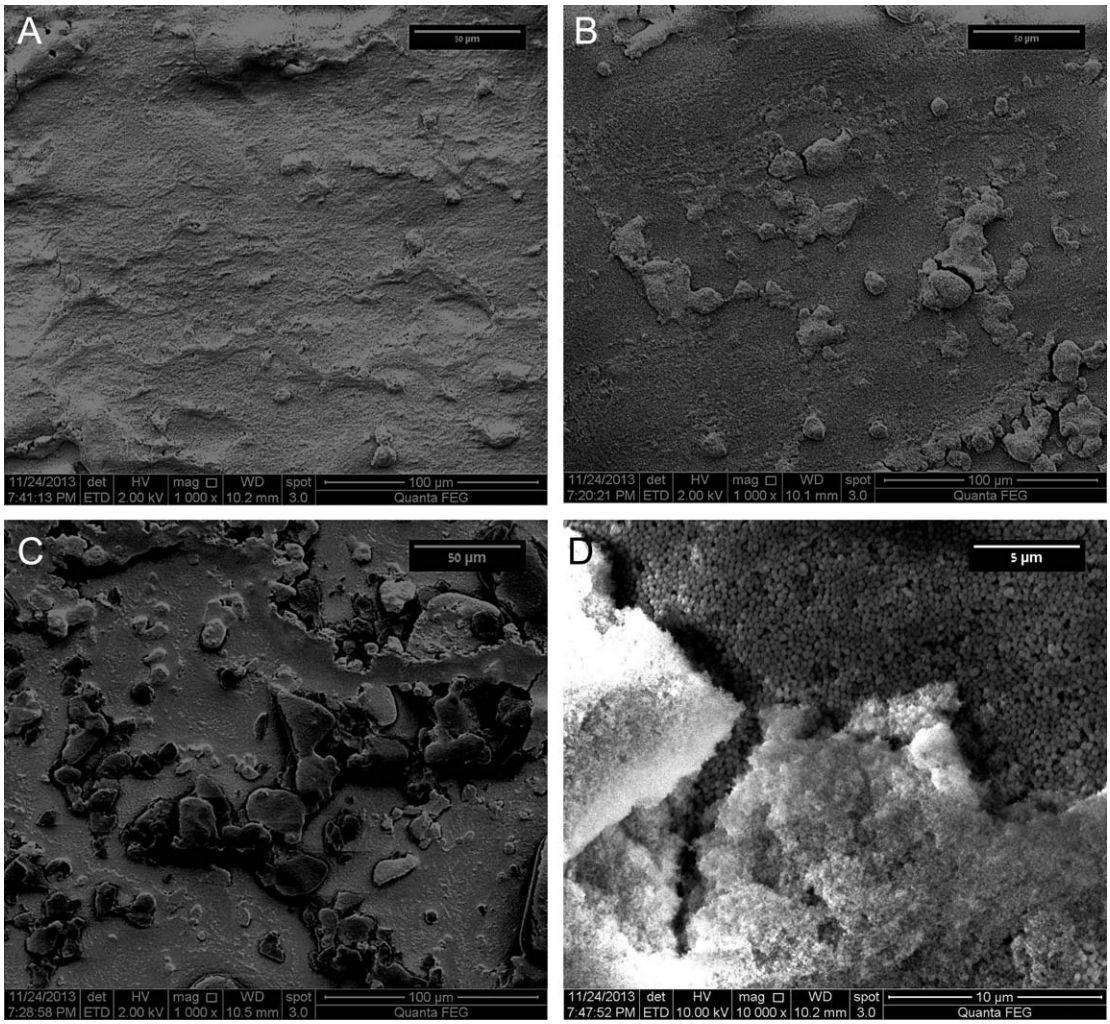

Figure 7. SEM topography image of A) FC294 after air flow test, B) FC156 after air flow test, C) FC65 after air flow test, and D) magnification image of FC294 after air flow test.

measured by SEM. Results indicated that high contact angles and low sliding angles, were achieved when the spacing between the pillars was lower than the water droplets diameter. Wide spacing may cause the penetration of the water droplet into the microstructure depressions resulting in Wenzel state. As can be observed in Figure 5(A,E,H,K), the spacing between the pillars was much smaller compared to the water drops. The surface of the neat UA [Figure 5(A)] has a smooth appearance. The superhydrophobic surfaces containing four layers (5 B–D), exhibited non uniform spacing, with average distances between peaks shorter than 0.11 mm while the 5 and 30-µL water droplets, used in the study had 3.85 and 2.12 mm diameter, respectively.

To evaluate of the shear resistance of the multilayer superhydrophobic coatings an air drag test was devised using an air gun with air velocity of 300 km/hr. The CAs and SAs were measured before and after the air drag test and are given in Figure 6(A,B). FC294, FC156, and FC65 were designated as the coatings containing SiO_2@BPh NPs of 294, 156, and 65 nm, respectively. As could be concluded the contact angle measurements showed insignificant changes in all coatings before and after air flow. However, an increase in sliding angles was observed after air drag. Both FC294 and FC156 kept their superhydrophobicity demonstrating SA smaller than 10° after the air drag test while FC65 exhibited a SA above 30°. These results might be explained by detachment of the nonbonded hydrophobic methylated fumed silica exposing the hydrophilic SiO_2@BPh NPs to the surface. As a result an increase in contact area between the water drops and polymer substrate was obtained moving from Cassie to Wenzel state. SEM images [Figure 7(A,B)] showed a slight decrease in surface roughness for FC294 and FC156 containing compositions which explain the slight increase in SA. However, a close look on FC294 containing coating [Figure 7(D)] confirmed that surface roughness was kept and the

Table I. Calculated Drag Force and Shear Stress as Function of Particle Size

Particle size (nm)	Drag Force (nN)	Shear Stress (MPa)
294	5.94	0.1
156	3.42	0.22
65	1.45	0.53

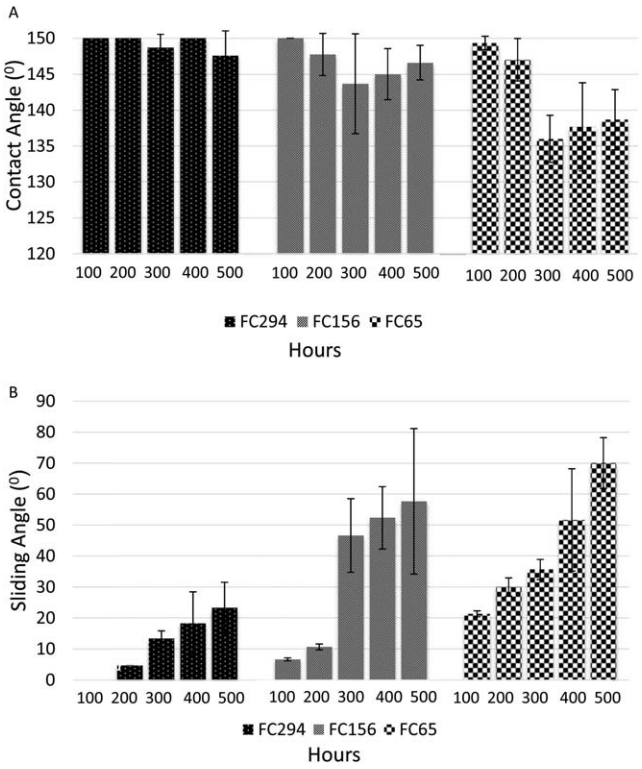

Figure 8. A) Contact angles results of FC294, FC156, and FC65 after 100 to 500 hr. B) Sliding angles results of FC294, FC156, and FC65 after 100 to 500 hr.

increase in sliding angle was a consequence of the loss of non-bonded methylated fumed silica in some areas. In FC65 containing coatings [Figure 7(C)], cracks could be noticed on the surface that led to the increase in SA.

To analyze the shear (drag) resistance of the bonded NPs, the shear stress applied on a single nanoparticle exposed to air velocity of 300 km/hr was calculated using eqs. (1) and (2). Results are summarized in Table I. As can be observed in Table I, larger particles (294 nm) developed higher drag resistance and low shear stress compared to smaller particles (65 nm) which is proportional to the contact area of the NP and the polymer layer. It should be mentioned that for good adhesion the shear stresses should be approximately 10 MPa, thus higher drag forces should be applied to evaluate the shear strength of the NPs to the surface polymer.

The accelarated UV/humidity stability attributes are shown in Figure 8(A,B). In general, all surfaces showed reduction in their superhydrophobic characteristics following exposure to the accelerated conditions with exposure time. This may be attributed to degradation of the base UA and other carbon–carbon bonds. Best durability was observed for the 294 nm NPs containing coatings having CA of 148° and SA of 23° after 500 hr exposure. The worst performance was observed for the low diameter 65 nm NPs containing coating that lost its superhydrophobic characteristics after 100 hr exposure. The FC156 containing coating kept its superhydrophobicity for the first 200 hr exposure. These results can be explained by the masking effect of SiO_2@BPh NPs inhibiting the UA degradation with increase of the NPs diameter.

CONCLUSIONS

In this work, the preparation of stable superhydrophobic coating was demonstrated by UV chemistry using silica NPs of various diameters grafted with photoreactive BP groups and methylated fumed silica NPs in combination with urethane acrylate base layer and Fluorosilane top layer. The coatings showed good air drag resistance (300 km/hr) to air. Accelerated weather conditions were used to evaluate outdoor durability.

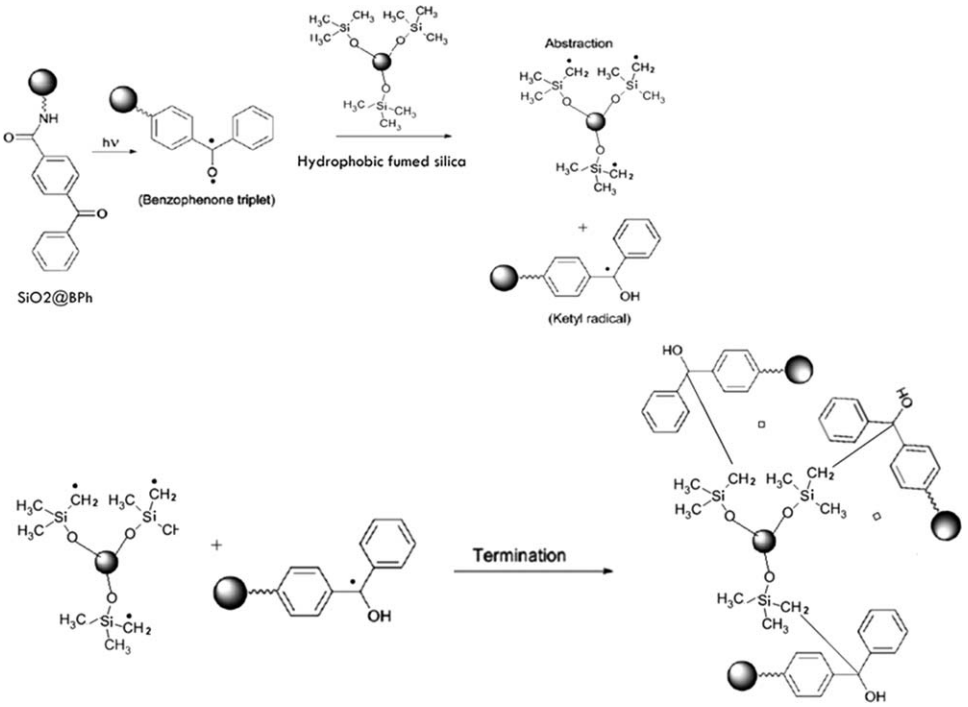

Scheme 2. Proposed mechanism for the photochemical reaction between SiO_2@BPh NPs and methylated fumed silica.

Best performance was observed when using photoreactive silica NPs with an average diameter of 294 nm. The methodology that was practiced can be applied for preparation of durable silica NPs based coatings comprised of various based polymers that can be activated by hydrogen abstraction mechanism.

REFERENCES

1. Cassie, A.; Baxter, S. *Trans. Faraday Soc.* **1944**, *40*, 546.
2. Institut, B.; Garten, B.; Allee, M. Characterization and Distribution of Water-repellent, Self-cleaning Plant Surfaces. *Annals of Botany* **1997**, *79*, 667.
3. Rios, P. F.; Dodiuk, H.; Kenig, S.; Mccarthy, S.; Dotan, A. *Polym. Adv. Technol.* **2008**, *19*, 1684.
4. Chen, Y.; Chen, S.; Yu, F.; Sun, W.; Zhu, H.; Yin, Y. *Surf. Interface Anal.* **2009**, *41*, 872.
5. Cheng, J.; Yang, Z. R.; Hai, J.; Yang, J. X. *Adv. Mater. Res.* **2011**, *328–330*, 1263.
6. Seo, H. O.; Kim, K.-D.; Jeong, M.-G.; Kim, Y. D.; Choi, K. H.; Hong, E. M.; Lee, K. H.; Lim, D. C. *Macromol. Res.* **2011**, *20*, 216.
7. Wang, Z.; Li, Q.; She, Z.; Chen, F.; Li, L. *J. Mater. Chem.* **2012**, *22*, 4097.
8. Dikić, T.; Ming, W.; van Benthem, R. a T. M.; Esteves, a C. C.; de With, G. *Adv. Mater.* **2012**, *24*, 3701.
9. Alizadeh, A.; Yamada, M.; Li, R.; Shang, W.; Otta, S.; Zhong, S.; Ge, L.; Dhinojwala, A.; Conway, K. R.; Bahadur, V.; Vinciquerra, A. J.; Stepheness, B.; Blohm, M. L. *Langmuir* **2012**, *28*, 3180.
10. Kulinich, S. a.; Farhadi, S.; Nose, K.; Du, X. W. *Langmuir* **2011**, *27*, 25.
11. Dotan, A.; Dodiuk, H.; Laforte, C.; Kenig, S. *J. Adhes. Sci. Technol.* **2009**, *23*, 1907.
12. Farhadi, S.; Farzaneh, M.; Kulinich, S. a. *Appl. Surf. Sci.* **2011**, *257*, 6264.
13. Saito, H.; Takai, K. *Surf. Coat. Int. Part B Coat. Trans.* **1997**, *80*, 168.
14. Du, L. U.; Chicoutimi, Q. À.; Partielle, C. E.; Maîtrise, D. E. L. A.; Ingénierie, E. N. Water and ice-repellent properties of nanocomposite coatings based on silicone rubber Propriétés hydrophobes et glaciophobes de revêtements nanocomposites à base de silicone. Master Thesis Universite du Quebec a Chicoutimi (Canada) **2010**.
15. Bhushan, B. *Langmuir* **2012**, *28*, 1698.
16. Roach, P.; Shirtcliffe, N. J.; Newton, M. I. *Soft Matter* **2008**, *4*, 224.
17. Zhang, Z.; Zhang, T.; Zhang, Y. W.; Kim, K.-S.; Gao, H. *Langmuir* **2012**, *28*, 2753.
18. Cao, L. Superhydrophobic surfaces: Design, Fabrication, and applications. PhD Thesis, Graduate Faculty of Swanson School of Engineering, Chemical Engineering, University of Pittsburgh. **2010**.
19. Zhang, B.; Wang, J.; Zhang, X. *Langmuir* **2013**, *29*, 6652.
20. Bhushan, B.; Jung, Y. C. *Prog. Mater. Sci.* **2011**, *56*, 1.
21. Gao, J.; Li, Y.; Li, Y.; Liu, H.; Yang, W. *Cent. Eur. J. Chem.* **2012**, *10*, 1766.
22. Youngblood, J. P.; McCarthy, T. *J. Macromolecules* **1999**, *32*, 6800.
23. Feng, J.; Tuominen, M. T.; Rothstein, J. P. *Adv. Funct. Mater.* **2011**, *21*, 3715.
24. Shiu, J.; Kuo, C.; Chen, P. *Chem. Mater.* **2004**, *16*, 561.
25. Mahadik, S.; Mahadik, D. B.; Kavale, M. S.; Parale, V. G.; Wagh, P. B.; Barshilia, H. C.; Gupta, S. C.; Hegde, N. D.; Rao, A. V. *J. Sol-Gel Sci. Technol.* **2012**, *63*, 580.
26. Xu, Q. F.; Wang, J. N.; Smith, I. H.; Sanderson, K. D. *J. Mater. Chem.* **2009**, *19*, 655.
27. Pi, P.; Mu, W.; Fei, G.; Deng, Y. *Appl. Surf. Sci.* **2013**, *273*, 184.
28. Ogihara, H.; Xie, J.; Okagaki, J.; Saji, T. *Langmuir* **2012**, *28*, 4605.
29. Zhang, X.; Shi, F.; Yu, X.; Liu, H.; Fu, Y.; Wang, Z.; Jiang, L.; Li, X. *J. Am. Chem. Soc.* **2004**, *126*, 3064.
30. Rahmawan, Y.; Xu, L.; Yang, S. *J. Mater. Chem. A* **2013**, *1*, 2955.
31. Yilgor, I.; Bilgin, S.; Isik, M.; Yilgor, E. *Polymer* **2012**, *53*, 1180.
32. Peng, C.-W.; Chang, K.-C.; Weng, C.-J.; Lai, M.-C.; Hsu, C.-H.; Hsu, S.-C.; Li, S.-Y.; Weib, Y.; Yeh, J.-M. *Polym. Chem.* **2013**, *4*, 926.
33. Hwang, H. S.; Lee, S. B.; Park, I. *Mater. Lett.* **2010**, *64*, 2159.
34. Jin, M.; Feng, X.; Feng, L.; Sun, T.; Zhai, J.; Li, T.; Jiang, L. *Adv. Mater.* **2005**, *17*, 1977.
35. Lee, S. E.; Lee, D.; Lee, P.; Ko, S. H.; Lee, S. S.; Hong, S. U. *Macromol. Mater. Eng.* **2013**, *298*, 311.
36. Sun, W.; Zhou, S.; You, B.; Wu, L. *J. Mater. Chem. A* **2013**, *1*, 3146.
37. Verho, T.; Bower, C.; Andrew, P.; Franssila, S.; Ikkala, O.; Ras, R. H. A. *Adv. Mater.* **2011**, *23*, 673.
38. Xiu, Y.; Liu, Y.; Hess, D. W.; Wong, C. P. *Nanotechnology* **2010**, *21*, 155705.
39. Xiu, Y.; Liu, Y.; Balu, B.; Hess, D. W. Wong, C. *IEEE Trans. Compon Package Manuf. Technol.* **2012**, *2*, 395.
40. She, Z.; Li, Q.; Wang, Z.; Li, L.; Chen, F.; Zhou, J. *Chem. Eng. J.* **2013**, *228*, 415.
41. Xiu, Y.; Hess, D. W.; Wong, C. P. *J. Colloid Interface Sci.* **2008**, *326*, 465.
42. Zimmermann, J.; Rabe, M.; Artus, G. R. J.; Seeger, S. *Soft Matter* **2008**, *4*, 450.
43. Zhai, L.; Berg, M.C.; Cebeci, F.; Kim,Y.; Milwid, J. M.; Rubner, M. F.; Cohen, R. E. *Nano Lett.* **2006**, *6*, 1213.
44. Papadopoulos, P.; Mammen, L.; Deng, X.; Vollmer, D.; Butt, H.-J. *Proc. Natl. Acad. Sci. USA.* **2013**, *110*, 3254.
45. Nahum, T.; Dodiuk, H.; Dotan, A.; Kenig, S.; Lellouche, J.-P. *Polym. Adv. Technol.* **2014**, *25*, 723.
46. Peled, A.; Naddaka, M.; Lellouche, J.-P. *J. Mater. Chem.* **2011**, *21*, 11511.
47. Hoerner, D. I. S. In Fluid-Dynamic Drag: Theoretical, experimental and statistical information by Hoerner, Dr. Ing. S.F.: Hoerner Fluid Dynamics Hardcover, 2nd ed.; Warrior Books, **1965**.
48. Zhao, H.; Park, K.-C.; Law, K.-Y. *Langmuir* **2012**, *28*, 14925.